Results in Physics 51 (2023) 106676

Contents lists available at ScienceDirect

Results in Physics

journal homepage: www.elsevier.com/locate/rinp

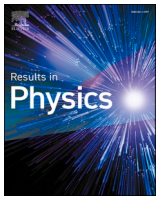

# Endo/exothermic chemical processes influences of tri-hybridity nanofluids flowing over wedge with convective boundary constraints and activation energy

Tanveer Sajid [a], Mohammed K. Al Mesfer [b], Wasim Jamshed [a], Mohamed R. Eid [c,d], Mohd Danish [b], Kashif Irshad [e], Rabha W. Ibrahim [f,g,h], Sawera Batool [i,*], Sayed M. El Din [j], Gilder Cieza Altamirano [k,l]

[a] Department of Mathematics, Capital University of Science and Technology (CUST), Islamabad 44000, Pakistan
[b] Chemical Engineering Department, College of Engineering, King Khalid University, Abha, Saudi Arabia
[c] Department of Mathematics, Faculty of Science, New Valley University, Al-Kharga, Al-Wadi Al-Gadid 72511 Egypt
[d] Department of Mathematics, Faculty of Science, Northern Border University, Arar 1321, Saudi Arabia
[e] Interdisciplinary Research Centre for Renewable Energy and Power System (IRC-REPS), Research Institute, King Fahd University of Petroleum and Minerals (KFUPM), Dhahran 31261, Saudi Arabia
[f] Near East University, Mathematics Research Center, Department of Mathematics, Near East Boulevard, PC:99138 Nicosia, Mersin 10, Turkey
[g] Department of Computer Science and Mathematics, Lebanese American University, Beirut, Lebanon
[h] Information and Communication Technology Research Group, Scientific Research Center, Al-Ayen University, Thi-Qar, Iraq
[i] Department of Physics, Benazir Bhutto Shaheed University (BBSU), Peshawar 25000, Pakistan
[j] Center of Research, Faculty of Engineering, Future University in Egypt New Cairo, 11835, Egypt
[k] Universidad Nacional Autónoma de Chota, Cajamarca, Perú
[l] Fizmako Research Group, Bogotá, Colombia

ARTICLE INFO

*Keywords:*
Trihybrid nanofluid
Prandtl Eyring fluid
Wedge geometry
Variant thermal conductivity
Active energy

ABSTRACT

Prandtl Eyring fluid and stretchable wedge have multiple usages in many industries. The present study aims to investigate the impact of modified Buongiorno trihybrid nanofluid on Prandtl Eyring fluid past a wedge with the addition of various influences like endothermic/exothermic reactions, thermal radiation, and thermal conductivity, Cattaneo-Christov double diffusion. Aluminium alloys (*AA7072*), Aluminium alloys (*AA7075*) and Silver (*Ag*) are used as nanocomponents. Prandtl Eyring fluid is employed as a conventional liquid in the preparation of nanofluids by blending nano components into the base fluid. Further, the flow model is imposed with Modified Buongiorno nanofluid. By using the similarity approach, the proposed mathematical flow model of partial differential equations (PDEs) is turned into highly nonlinear ordinary differential equations (ODEs). Throughout the whole range of material parameters, the solution for the ensuing nonlinear boundary value issue is given by employing the finite element method (FEM). The numerical results of Prandtl Eyring ternary HNF motion, thermal and solute profiles are performed through graphical amassment on the collected data and discussed in detail. The numerical significances of material sections, such as the frictional force, local Nusselt quantity, and local Sherwood number requirements, are supplied in tabular form. Further, it also presents the validation and performance characteristics of the proposed device with previously published work and found excellent accuracy. In comparison to hybrid nanoparticles, the consequences reveal that heat transmission is amplified in the case of tri-hybrid nanoparticles. The numerical consequences show that the heat transfer amount reduces in the situation of exothermic reactions parameter $\Omega < 1$ and rises due to magnification in the status of endothermic reactions parameter $\Omega > 1$.

* Corresponding author.
*E-mail address:* saweraktk@hotmail.com (S. Batool).

https://doi.org/10.1016/j.rinp.2023.106676
Received 4 April 2023; Received in revised form 13 June 2023; Accepted 22 June 2023
Available online 28 June 2023

**Nomenclature**

| | |
|---|---|
| $A$ | Prandtl fluid parameter |
| $T_w$ | wall temperature $(K)$ |
| $\gamma_1$ | buoyancy parameter $(N)$ |
| $Q$ | Activation energy $\left(\frac{kJ}{mol}\right)$ |
| $U_e$ | Free streaming rapidity |
| $Nb$ | Brownian diffusion $\left(\frac{m^2}{s}\right)$ |
| $Pr$ | Prandtl number |
| $\beta_1$ | Reaction rate constant |
| $D$ | Convective heat flux $\left(\frac{W}{m^2.K}\right)$ |
| $\lambda$ | Moving wedge parameter |
| $\rho_{thnf}$ | Density of nanofluid $\left(\frac{Kg}{m^3}\right)$ |
| $C_p$ | Specific heat $\left(\frac{J}{kg.K}\right)$ |
| $\sigma^*$ | Stefan-Boltzmann constant $\left(\frac{W}{m^2.K^4}\right)$ |
| $B$ | elastic parameter |
| $T_\infty$ | ambient temperature $(K)$ |
| $m$ | wedge parameter |
| $n$ | Power law index $\left(\frac{kg}{m.s}\right)$ |
| $U_w$ | Rapidity at wall |
| $Nt$ | Thermophoresis parameter |
| $Rd$ | radiation parameter |
| $\Omega$ | Endothermic/exothermic reaction |
| $Z$ | Convective mass flux $\left(\frac{kg}{m^2.s}\right)$ |
| $\alpha$ | Wedge angle $(Rad)$ |
| $\alpha_{thnf}$ | Thermal diffusivity of tri-hybrid mixture $\left(\frac{m^2}{s}\right)$ |
| $k_{thnf}$ | Thermal conductivity of nanofluid $\left(\frac{J}{kg.K}\right)$ |
| $\kappa^*$ | absorption coefficient $\left(\frac{m^2}{mol}\right)$ |

## Introduction

It is difficult to accurately forecast the precise nature of non-Newtonian fluids because of the intricate interaction that exists between the shearing stress and the strain that is exerted. Various mathematical prototypes have been developed based on viscoelastic, rheopectic, thixotropic, and dilatant behaviors. Unlike Newtonian fluids, non-Newtonian fluids do not follow the third law of motion. Viscosity in Newtonian fluids is constant because shear stress is proportional to strain. Oil extraction, biochemicals, medicines, foods, and power engineering are only a few of the fields where non-Newtonian fluids have been explored. Non-Newtonian fluids include things like synthetic and natural liquid organisms, polymers, emulsions, paints, blood, oil, toothpaste, and ketchup. As compared to Newtonian fluids, non-Newtonian fluids are more challenging to control numerically and analytically due to their complexity and nonlinearity. Carreau studied the initial formulation of the stress tensor to characterize the nonlinear and viscoelastic characteristics of non-Newtonian fluids. Pseudoplastic fluids that are thin under shear have important applications. The viscosity of a fluid drops as shear stress increases. Blood is a typical instance of this. Models of fluids that are thin in shear have been developed. Because of its ability to accurately portray decreased shear fluids, the Prandtl fluid model is significant. Researchers from all over the globe have conducted studies on the impact of numerous events on non-Newtonian fluids in order to examine heat and mass transfer analyses. This is because non-Newtonian fluids have a complicated character.

The non-Newtonian character of blood flowing in multi-stenosed arteries with an oval cross-section is investigated and understood by Shahzad et al. [1]. The Carreau fluid concept takes into account the fact that blood does not behave in a Newtonian manner. Raza et al. [2] researched Burgers' fluid, which is of the transient electro-osmotic kind. Their experiment took place in a tiny tube with a circular cross-section. Shahzad and Awan. [3] presented the analytical study of the peristaltic flow of heated non-Newtonian Rabinowitsch fluid flow subjected to an elliptical duct. Shahzad and Awan. [4] taken Phan-Thein–Tanner fluid model in order to investigate the effect of blood flowing in a contaminated vein with an elliptical cross-section. Impression of magnetism force and Darcy- Forchheimer flow on Casson liquid flow across a circular cylinder was investigated in detail by Awan et al. [5]. Shah et al. [6] studied the impact of activation energy and magnetic field on thermally radiated bioconvective Prandtl fluid flow towards an expandable cylinder. The effect of Coriolis force and nanoparticles on rotating Prandtl fluid was elaborated in the description by Awan et al. [7]. Shah et al. [8] investigated the influence of free convection on viscid liquid flow under the effect of an oblique magnetism force. Li et al. [9] investigated the effect of thermal radiation and viscous dissipation on chemically reactive time-dependent fluid flow across an elastic sheet. The effects of buoyancy on nanofluid flow exposed to a slippery were probed deeply by Liu et al. [10]. Chu et al. [11] scrutinized the effect of activation energy and double diffusion convection of magnetized tangent hyperbolic fluid. The buoyancy effect along with stagnation point flow on the Carreau fluid-embedded Catteneo-Christov heat flux phenomenon was studied deeply by Li et al. [12]. Chemically reactive squeezed Casson fluid accompanied by activation energy and viscous dissipation past a horizontal channel were interrogated in the description by Li et al. [13]. Li et al. [14] elaborated on the influence of Thomson and Troian slip phenomena on ternary nanofluid via a stretchable plate. Similar works reported by various researchers for authors' interest are mentioned in Refs. [14–18].

The boundary layer flowing of any classical/nanofluids over the wedge is a modern problem in computational fluid dynamics, and this type of phenomenon is observed in many processes such as submarines, warship modelling, designing flaps on aeroplane wings, nuclear power plants, cooling air through AC panels, liquid metal flows in heat exchangers, crude oil extraction, and polymer processing. Moreover, the wedge angle plays an important role in airfoils and wings in transonic flows. The study of nano-liquid motion past a moving plate has several implementations like cooling the electronic device, drying technology, heat exchanger, solar energy storage, biomedical devices, atmospheric flow, and polymer processing. Keeping these facts, many investigators started working on diverse nano-liquid motions over the static/moving wedge. For instance, Anuar et al. [19] have presented bvp4c solutions to investigate the alumina oxide-copper/water nanofluid flowing via a moving wedge and concluded that boundary layer separation is delayed by the wedge parameter. Mishra et al. [20] have presented a theoretical analysis of the boundary layer motion of nano-liquid over a wedge and noticed that heat sinking blankets the surface with the cold fluid layer. Khan and Pop [21] have provided the Keller-box method solutions to examine the boundary layer motion of nanoliquid via a wedge and concluded that the wedge parameter decreases the thickness of hydrodynamic thickness. Dharmaiah et al. [22] examined the MHD nanofluid movement via a wedge underneath the Ohmic effects with the bvp4c procedure and accomplished that their solutions may be helpful in polymeric sheets, plastic film, and wire drawing. Sarkar and Endalew [23] have provided collocation-based solutions for the MHD wedge motion of a Casson nano-liquid through a porous medium and concluded that their findings may be helpful in designing cooling gadgets and heat sinks. Khan et al. [24] elaborated the Carreau nanoliquid motion over

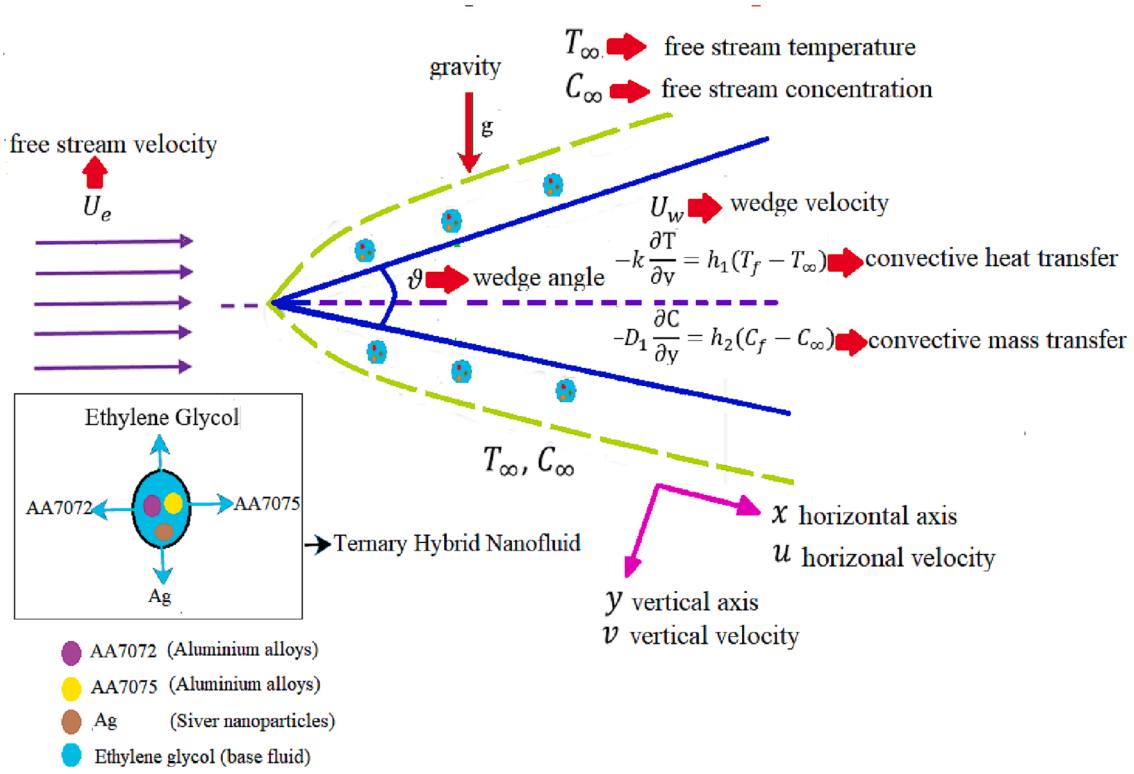


**Fig. 1.** Geometry of the fluid flow.

the wedge with mass flux and non-linear radiation effects using MATLAB package and provided that the lower velocities are found in the case of the static wedge and the higher velocities are noticed in the moving wedge. Madhu et al. [25] have offered numerical finite element (FM) results for the MHD Sisko nanofluid motion past a wedge and discussed the salient features. Kebede et al. [26] have investigated the motion of tangent hyperbolic nanoliquid via a stretchable wedge using the computational software Mathematica and found that by developing the value of wedge angle the velocity rises. Rajput et al. [27] have discussed the 2D unsteady motion of HNF over a wedge using the bvp4c approach and concluded that heat and mass transfer rate and skin-friction coefficients noticeably change for favorable and adverse pressure conditions. Madhu and Kishan [28] have used FM method to probe the flowing situation of MHD nanoliquid via a wedge and provided that the wedge angle enhances the velocity profiles. Jabeen et al. [29] explored the motion of Casson nanoliquid past a wedge under the microorganism effects using the bvp4c procedure and noted that suction/injection performs a worthy position in controlling the boundary layer motion.

Over the last decades, the diverse HNFs boundary layer motion over the stretchable/shrinking wedge has established much consideration because of its practical applications in various fields such as glass blowing, artificial fiber, extraction of polymer, and paper production. These applications motivated the researchers to work on HNFs over the wedge. Dinarvand et al. [30] have used MATLAB software to investigate the motion of titanium oxide-copper oxide/water HNF over a wedge and concluded that the mono-nanofluid and base fluid has less thermal performance as compared with HNFs. Zainal et al. [31] have analyzed the motion of alumina oxide-copper/water HNF past a wedge using the computational software MATLAB and provided that their finding may be helpful in the thermal analysis process. Kakar et al. [32] have made a theoretical analysis of the water-based HNF over the shrinking wedge with MATLAB software and concluded that wedge angle enhances thermal boundary layer thickness. Zainal et al. [33] have studied the unsteady hybrid nano-material motion over the moving Falkner-Skan wedge using the bvp4c technique and found that wedge angle and dual-type nanoparticles improve thermal efficiency. Berrehal et al. [34] have discussed the motion of magnetite-graphene oxide/water HNF using the Runge-Kutta-Fehlberg method and concluded that their results are helpful in cooling technologies. Ogunniyi et al. [35] inspected MHD HNF flow via the wedge using the homotopy analysis method and declared that temperature increases with an increase in solid volume fraction. Waini et al. [36] have used MATLAB computational software to investigate the indication of hybrid nanomaterial done by the stretching wedge and determined that as compared with normal nanofluid, a higher heat transference rate is detected in HNF. Roșca et al. [37] have studied the HNF over a wedge and found that their findings are helpful in heat exchangers. Basha et al. [38] made a numerical investigation to discuss the motion of Ag-MgO/water HNF past a Riga wedge and noticed that the stronger magnetic field lowers the temperature distribution. Hassan et al. [39] have studied the motion of copper-silver/water HNF over the wedge and concluded that the efficacy of HNFs as a heat transference liquid is significantly supplementary to standard liquids.

*Motivation*

In the current examination, investigators have concentrated on the flow of ternary HNFs, which are made up of three dissimilar categories of nanoparticles floating in a base fluid. This idea is similar to the mono/ HNFs. In general, the ternary HNFs have more significant thermophysical properties than mono/ HNFs due to their synergistic effects. Nowadays, ternary HNFs are regarded as new-generation fluids; however, very little work has been done in the literature in the direction of ternary HNF flows in various situations; however, no effort is done in the case of Prandtl Eyring Ternary HNF flow with tri HNFs past a wedge.

*Objective*

With this motive, the authors of the current paper investigated the effect of modified ternary HNF flow across the wedge by taking into account numerous aspects such as activation energy, chemical processes, and multiple convective boundary conditions. The nanoparticles have been considered alumina oxide, titanium dioxide, and silicon

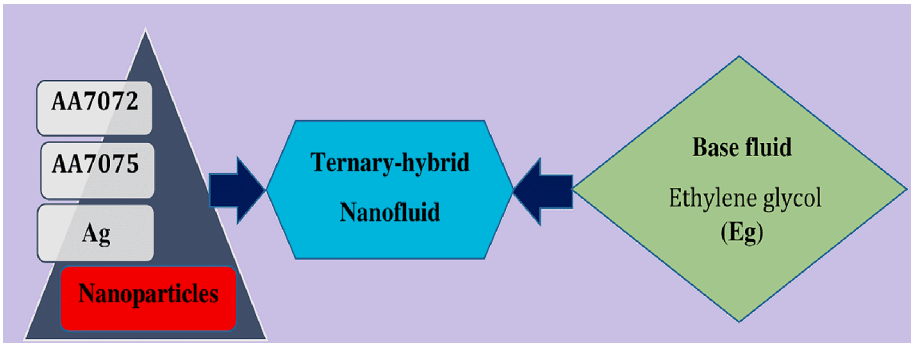


**Fig. 2.** Ternary HNFs.

dioxide in the base fluid. The mathematical model is developed and with suitable similarity transformations, the model is converted to a system of ODE's. The finite element methodology was managed to resolve the non-dimensional system of formulas. The graphical results for various parameters are then displayed.

*Novelty*

The motivation behind the conduct of the existing examination is given below.

1) The effect of tri-hybridity nanoparticles on fluid flowing via a wedge has never been elaborated on previously.
2) The modified di-hybrid Buongiorno nanofluid model is available in the existing literature. The novel idea of a modified tri-hybrid nanofluid Buongiorno nanofluid model is not implemented yet in the available literature.
3) In the previous literature, no attention has been paid to studying the influence of endothermic/exothermic chemically reactive processes on the liquid via a wedge.

*Applications*

The implementations of flowings via a wedge might be observed in the manufacturing of polymers, the extracting of petroleum products, the movement of boiling metals over accelerated surfaces, the movement of liquid metallic substances in heat exchange systems, the flinging of cold air through AC panels, nuclear power plants, the construction of the flaps on airplane wings for enhanced lift, drag, and maneuverability, the simulation of naval vessels and submersibles, and in a variety of other fields of scientific and technological research.

## Calculated description

In Fig. 1, the model of varied convective Prandtl Eyring fluid distributed with tri HNFs is carried out while taking into account ethylene glycol as a standard liquid. The heat transfer phenomenon is considered through the inclusion of endothermal (exothermal) responses and initiation energy. However, mass transfer investigation is explored under the light of initiation energy accomplish. With the use of variable thermal, conduction, radiate heat flow, and temperature variation are examined. When studying heat transmission, Rosseland radiative heat flux is taken into account. Considered is a modified Buongiorno HNF, which combines ternary HNF, Brownian diffusion, and thermophoresis phenomena. Heat and mass transport exploration have been elaborated with the insertion of the Cattaneo-Christov double diffusion phenomena. The factors $U_w$ and $U_e$ represent the extending velocity and ambient velocity. The heat as well as concentricity at the wall and ambient heat in accumulation to the concentricity are signified by $T_w$, $C_w$, $T_\infty$, $C_\infty$. Additionally, it is presumed that $T_w > T_\infty$ and $C_w > C_\infty$. The wedge is placed alongside $x-$ with $y-$ axes perpendicular to it. The gravity acceleration $g$ is smeared normal to the wedge route and moreover, the wedge angle is stated by $\vartheta$. The factors $\rho_{thnf}$, $(\rho C_p)_{thnf}$ and $k_{thnf}$ characterize the density, specific heat, and thermal conductivity of ternary HNF consistently. Above the consequence of boundary layer supposition, the properties like viscous dissipation and Joules's heating and mistreatment, and Boussinesq's approximation are measured since the buoyancy determined assorted convection affected that assumed in the momentum equation. Utilizing the Navier-Stokes equations, the 2nd-law of thermodynamics, Fick's 2nd-law of transmission, and the rule of conservation of mass, the continuity, energy, impetus, and concentricity formulas are produced. Because of the beyond suppositions, the influential formulas for continuity, impetus, energy, and concentration are provided further down.

Fig. 2 reflects the flowing diagram illustration of the ternary HNFs AA7072, AA7075, and Ag through the deliberation of ethylene glycol (EG) by means of a disreputable liquid in the current problem.

$$\frac{\partial u}{\partial x}+\frac{\partial v}{\partial y}=0, \tag{1}$$

$$u\frac{\partial u}{\partial x}+v\frac{\partial u}{\partial y}=U_e\frac{dU_e}{dx}+\frac{\mu_{thnf}}{\rho_{thnf}}\left[\frac{L}{C_1}\frac{\partial^2 u}{\partial y^2}+\frac{L}{2C_1^3}\left(\frac{\partial u}{\partial y}\right)^2\frac{\partial^2 u}{\partial y^2}\right]+\frac{1}{\rho_{thnf}}[g\beta(T-T_\infty)+g\beta^*(C-C_\infty)]\frac{Sin\vartheta}{2}, \tag{2}$$

$$u\frac{\partial T}{\partial x}+v\frac{\partial T}{\partial y}+\lambda_T\left[u^2\frac{\partial^2 T}{\partial x^2}+v^2\frac{\partial^2 T}{\partial y^2}+\left(u\frac{\partial u}{\partial x}+v\frac{\partial u}{\partial y}\right)\frac{\partial T}{\partial x}+2uv\frac{\partial^2 T}{\partial x\partial y}+\left(u\frac{\partial u}{\partial x}+v\frac{\partial u}{\partial y}\right)\frac{\partial T}{\partial y}\right]=\frac{\partial}{\partial y}\left(\frac{k_{thnf}}{(\rho C_p)_{thnf}}\frac{\partial T}{\partial y}\right)+\tau\left[D_B\frac{\partial C}{\partial y}\frac{\partial T}{\partial y}+\frac{D_T}{T_\infty}\left(\frac{\partial T}{\partial y}\right)^2\right]-\frac{1}{(\rho C_p)_{thnf}}\frac{\partial q_r}{\partial y}+\frac{\Omega k_r^2(C-C_\infty)\left(\frac{T}{T_\infty}\right)^n Exp\left(\frac{-Q_a}{\kappa T}\right)}{(\rho C_p)_{thnf}} \tag{3}$$

$$u\frac{\partial C}{\partial x}+v\frac{\partial C}{\partial y}+\lambda_C\left[u^2\frac{\partial^2 C}{\partial x^2}+v^2\frac{\partial^2 C}{\partial y^2}+\left(u\frac{\partial u}{\partial x}+v\frac{\partial u}{\partial y}\right)\frac{\partial C}{\partial x}+2uv\frac{\partial^2 C}{\partial x\partial y}+\left(u\frac{\partial u}{\partial x}+v\frac{\partial u}{\partial y}\right)\frac{\partial C}{\partial y}\right]=D_B\left(\frac{\partial^2 C}{\partial y^2}\right)+\frac{D_T}{T_\infty}\left(\frac{\partial^2 T}{\partial y^2}\right)-k_r^2(C-C_\infty)\left(\frac{T}{T_\infty}\right)^n\exp\left(\frac{-Q_a}{\kappa T}\right). \tag{4}$$

The following are the corresponding boundary restrictions:

**Table 1**
Thermophysical possessions.

| Properties | Ethylene Glycol (EG) | AA7072 | AA7075 | Ag |
|---|---|---|---|---|
| $\rho$ | 1114 | 2720 | 2810 | 10,500 |
| $C_p$ | 2415 | 893 | 960 | 235 |
| $k$ | 0.252 | 222 | 173 | 429 |

$$\left.\begin{aligned} y=0: u=u_w(x)=U_w x^m, v=0, -k\frac{\partial T}{\partial y}=h_1(T_f-T_\infty), -D_1\frac{\partial C}{\partial y}=h_2(C_f-C_\infty), \\ y\to\infty: u\to U_e(x)=U_\infty x^m, T=T_\infty, C=C_\infty \end{aligned}\right\} \tag{5}$$

Here are some calculated formulations for ternary HNF's thermophysical properties.

$$\left.\begin{aligned} \mu_{thnf} &= \frac{\mu_f}{(1-\phi_1)^{2.5}(1-\phi_2)^{2.5}(1-\phi_3)^{2.5}}, \\ \rho_{thnf} &= (1-\phi_3)\{(1-\phi_2)[(1-\phi_1)\rho_f+\rho_1\phi_1]+\rho_2\phi_2\}+\rho_3\phi_3, \\ (\rho C_p)thnf &= (1-\phi_3)\left\{(1-\phi_2)\left[(1-\phi_1)(\rho C_p)_f+(\rho C_p)_{s_1}\phi_1\right]+(\rho C_p)_{s_2}\phi_2\right\}+(\rho C_p)_{s_3}\phi_3, \\ \frac{k_{thnf}}{k_{hnf}} &= \frac{k_3+2k_{hnf}+2\phi_3(k_3-k_{hnf})}{k_3+2k_{hnf}+\phi_3(k_{hnf}-k_3)}, \\ \frac{k_{hnf}}{k_{nf}} &= \frac{k_2+2k_{nf}+2\phi_2(k_2-k_{nf})}{k_2+2k_{nf}+\phi_2(k_{nf}-k_2)}, \quad \frac{k_{nf}}{k_f}=\frac{k_1+2k_f+2\phi_1(k_1-k_f)}{k_1+2k_f+\phi_1(k_f-k_1)}. \end{aligned}\right\} \tag{6}$$

Thermophysical possessions of AA7072, AA7075, and Ag nanoparticles and EG base fluid are offered in the next table: Table 1.

The factor for the Rosseland approximation is

$$q_r = -\frac{4\sigma^*}{3\kappa^*}\frac{\partial T^4}{\partial y}, \tag{7}$$

where $\sigma^*$ and $\kappa^*$ signify the Boltzmann number and the absorbing factor, correspondingly.

Currently, think appropriate transformations are listed below.

$$\left.\begin{aligned} \psi &= \left(\frac{2\nu x U_e x^m}{m+1}\right)^{\frac{1}{2}} f(\eta), \eta = \left(\frac{U_e x^m(m+1)}{2\nu x}\right)^{\frac{1}{2}} y, \\ \theta(\eta) &= \frac{T-T_\infty}{T_w-T_\infty}, \ \phi(\eta)=\frac{C-C_\infty}{C_w-C_\infty}. \end{aligned}\right\}$$

Eqs. (2)–(5) are transformed as an outcome of the foregoing transformation keen on the following non-dimensional given by:

$$Af''' + Bf''' + A_1A_2\frac{m+1}{2}ff'' + A_1A_2m(1-f'^2) + A_1\gamma_1(\theta+N\phi)\frac{Sin\alpha}{2} = 0, \tag{8}$$

$$\left.\begin{aligned} &\left[\left((1+\epsilon\theta)+\frac{Rd}{A3}\right)\theta' + \epsilon\theta'^2\right] + \frac{A_3}{A_4}Pr\left(N_b\theta'\phi' + N_t\theta'^2\right) + \frac{1}{A_3}\Omega\beta_1(1+\delta\theta)^n exp\left(\frac{-Q}{1+\delta\theta}\right)\phi \\ &+\frac{A_3}{A_4}Prf\theta' - \frac{A_3}{A_4}Pr\Psi_1\left(\frac{m+1}{2}f'^2\theta' - \frac{6}{m+1}\eta f'^2\theta' + ff'\theta'\right) = 0, \end{aligned}\right\} \tag{9}$$

$$\begin{aligned} &\phi'' + \left(\frac{Nt}{Nb}\right)\theta'' + Scf\phi' - \beta_1 Sc(1+\delta\theta)^n exp\left(\frac{-Q}{1+\delta\theta}\right)\phi \\ &- Sc\Psi_2\left(\frac{m+1}{2}f'^2\phi' - \frac{6}{m+1}\eta f'^2\phi' + ff'\phi'\right) = 0, \end{aligned} \tag{10}$$

The endpoint preconditions (6) have the resulting structure:

$$\left.\begin{aligned} \eta=0: f(\eta)=0, f'(\eta)=\lambda, \theta'(0)=-D(1-\theta(0)), \phi'(0)=-Z(1-\phi(0)) \\ \eta\to\infty: f'(\eta)\to 1, \phi(\eta)\to 0, \theta(\eta)\to 0. \end{aligned}\right\} \tag{11}$$

**Physical measures**

The factors similar to drag constant $C_f$, heat transfer frequency $Nu_x$ and mass transfer ratio $Sh_x$ are

$$\left.\begin{aligned} C_f &= \frac{2\tau_w}{\rho_f u_w^2}, Nu_x = \frac{xq_w}{k_f(T_w-T_\infty)}, \end{aligned}\right\} \tag{12}$$

whereas expressions regarding $\tau_w$, $q_w$ and $q_m$ are given below

$$\left.\begin{aligned} \tau_w &= \mu_{nf}\left[\frac{A}{C_1}\frac{\partial u}{\partial y} + \frac{A}{2C_1^3}\left(\frac{\partial u}{\partial y}\right)^3\right] \\ q_w &= -k_{thnf}\left(\frac{\partial T}{\partial y}\right) + q_r. \end{aligned}\right\} \tag{13}$$

By substituting Eq. (17) for Eq. (16) and performing the comparing conversion, the quantities that are described in Eq. (17) be non-dimensional in the following way:

$$\left.\begin{aligned} \frac{1}{2}C_f Re^{1/2} &= \frac{1}{A_1}\left[\alpha f''' + \beta f'^3\right], \\ Nu_x Re_x^{-1/2} &= -(A_4+Rd)\theta'. \end{aligned}\right\} \tag{14}$$

where $Re_x = \frac{U_w x}{\nu_f}$. The following dimensionless parameters are derived from (10)-(13):

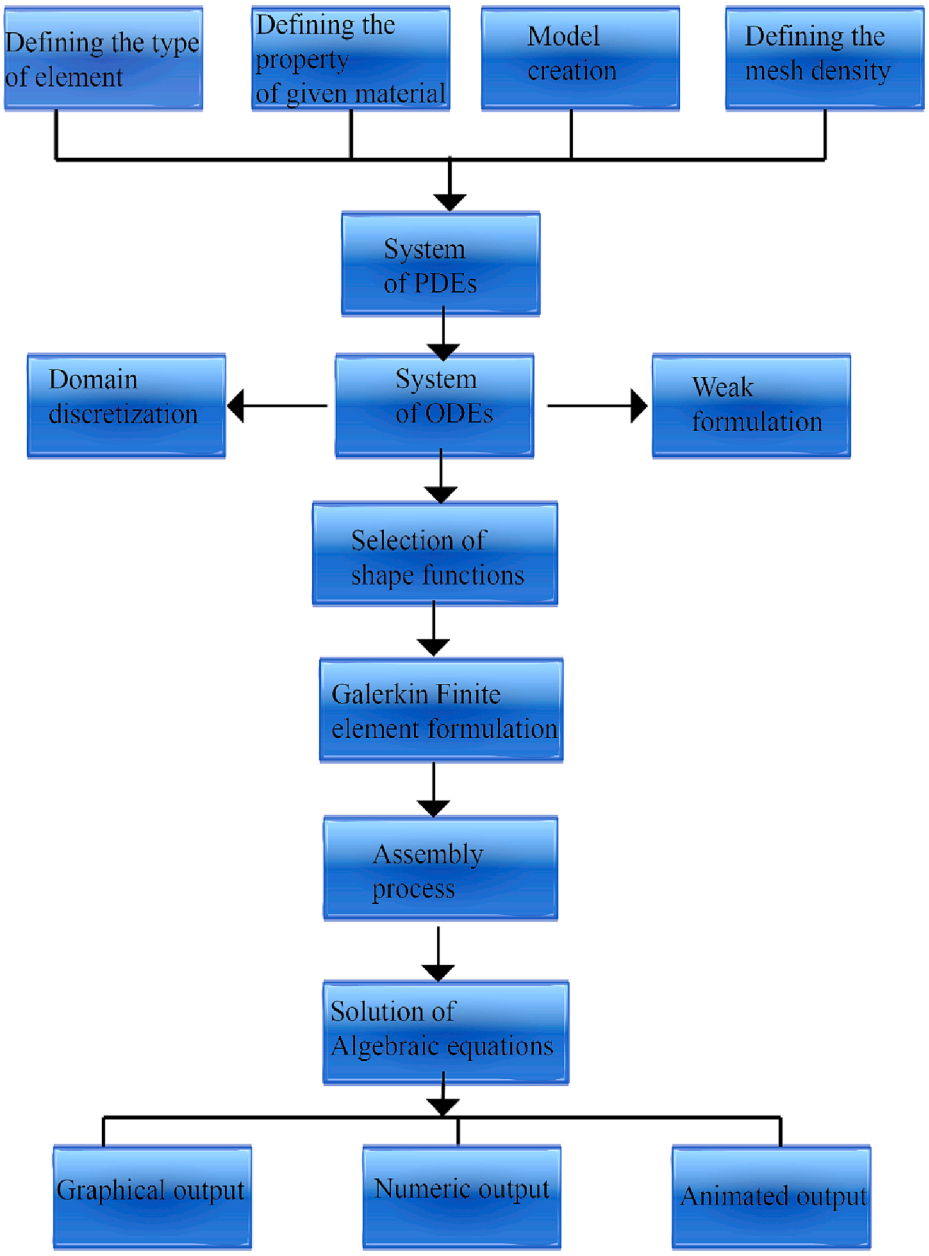


**Fig. 3.** G-FEM flow diagram.

$$\left.\begin{aligned}
&\lambda=\frac{U_w}{U_\infty},\ A=\frac{L}{\mu_f C_1},\ B=\left(\frac{L}{2C_1^2}\right)\left(\frac{(m+1)U_e^3 x^{m-1/3}}{2\nu_f}\right),\\
&Pr=\frac{\mu C_p}{k_\infty},\ R_d=\frac{16\sigma T_\infty^3}{3k^* k_\infty},\gamma_1=\frac{Gr_x}{Re_x^2},Gr_x=\frac{g\beta_T(T_w-T_\infty)x^3}{\nu_f^2}\\
&Q=\left(\frac{Q_a}{kT_\infty}\right),\ \delta=\frac{T_w-T_\infty}{T_\infty},\ Nb=\frac{\tau D_B}{\nu_f}(C_w-C_\infty),\\
&\beta_1=\sigma k_r^2,\ Nt=\frac{D_T}{T_\infty}\frac{\tau}{\nu_f}(T_w-T_\infty),\ \tau=\frac{(\rho C_p)_s}{(\rho C_p)_f},\\
&Sc=\frac{\nu_f}{D_B},\ \Psi_1=\lambda_T\frac{U_e}{2x},\ \Psi_2=\lambda_C\frac{U_e}{2x},
\end{aligned}\right\}$$

here $A_1$, $A_2$, $A_3$ and $A_4$ are assumed via

**Table 2**
Associating of $-\theta'(0)$ standards with $P_r$, when $\epsilon = 0$, $\phi = 0$, $\phi_{thnf} = 0$, $Nb = 0$, $Nt = 0$, $\lambda = 0$, $Z\to\infty$. and $D\to\infty$.

| *Pr* | Das et al [41] | Bouslimi et al. [42] | Present Results |
|---|---|---|---|
| $72 \times 10^{-2}$ | 0.80876122 | 0.80876181 | 0.80876181 |
| $1 \times 10^{0}$ | 1.00000000 | 1.00000000 | 1.00000000 |
| $3 \times 10^{0}$ | 1.92357431 | 1.92357420 | 1.92357420 |
| $7 \times 10^{0}$ | 3.07314679 | 3.07314651 | 3.07314651 |
| $10 \times 10^{0}$ | 3.72055436 | 3.72055429 | 3.72055429 |

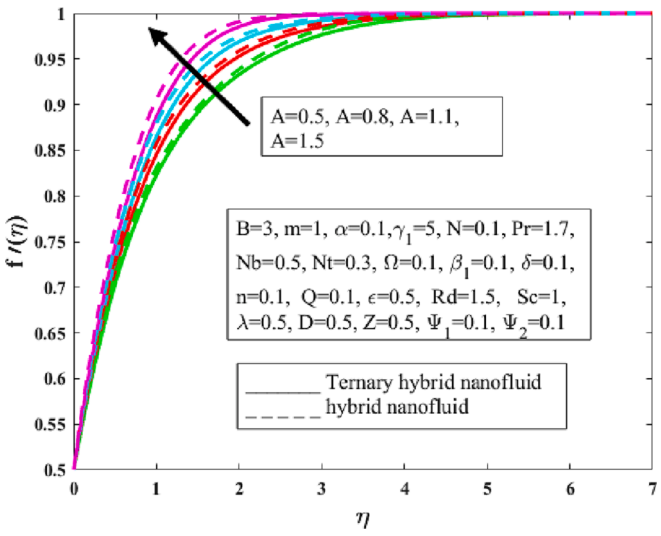


**Fig. 4.** Investigation of $A$ arranged by $f'(\eta)$.

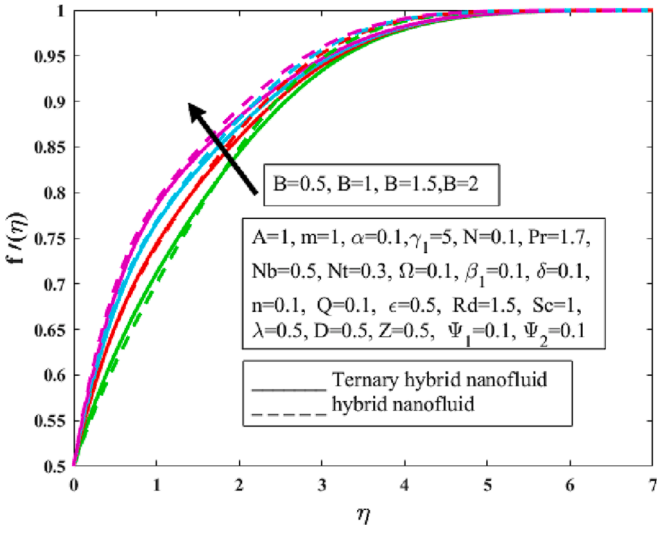


**Fig. 5.** Investigation of $B$ proceeding by $f'(\eta)$.

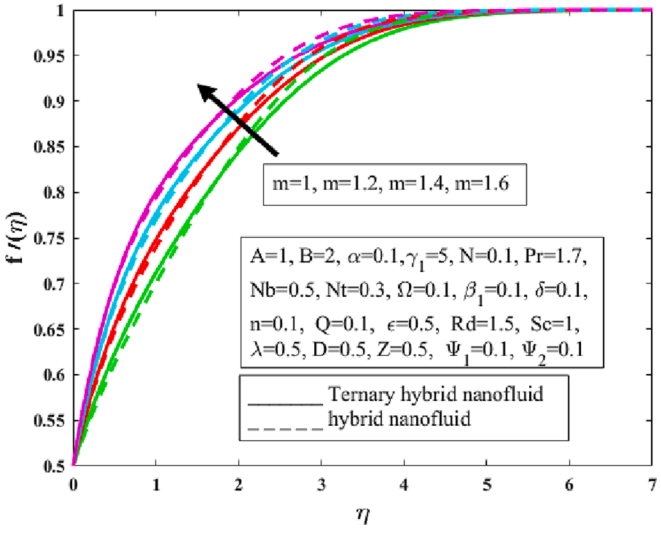


**Fig. 6.** Investigation of $m$ continuously by $f'(\eta)$.

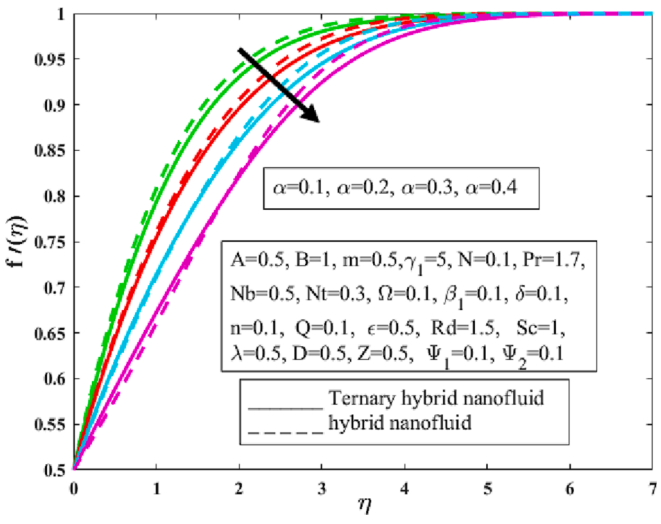


**Fig. 7.** Investigation of α scheduled by $f'(\eta)$.

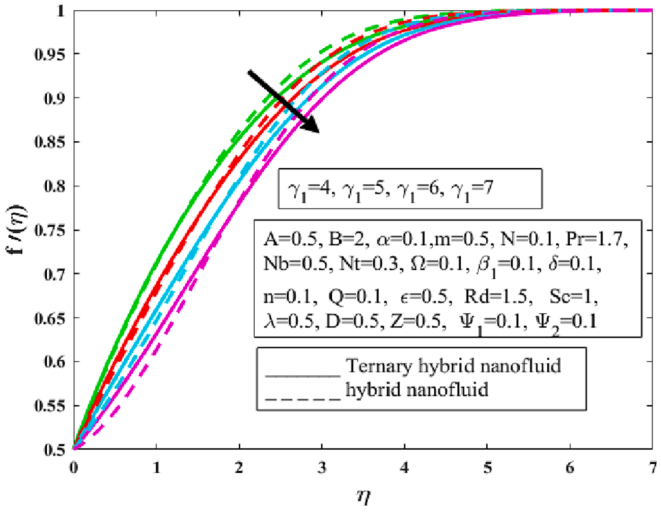


**Fig. 8.** Investigation of $\gamma_1$ proceeding by $f'(\eta)$.

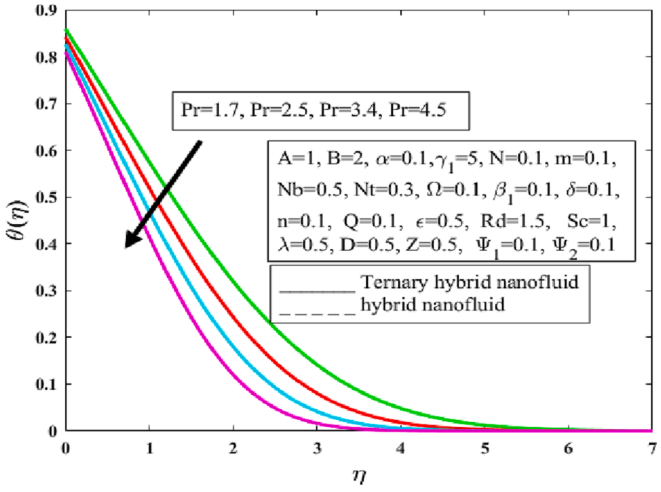


**Fig. 9.** Investigation of $Pr$ arranged by $\theta(\eta)$.

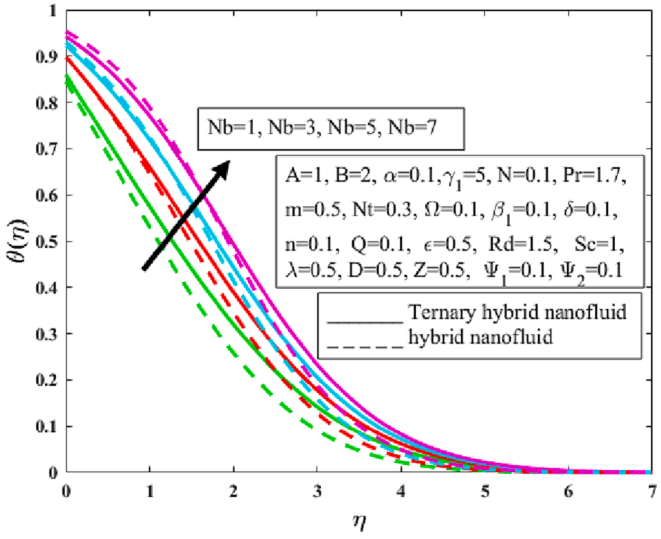


**Fig. 10.** Investigation of *Nb* indicated by[03*B*8]$(\eta)$.

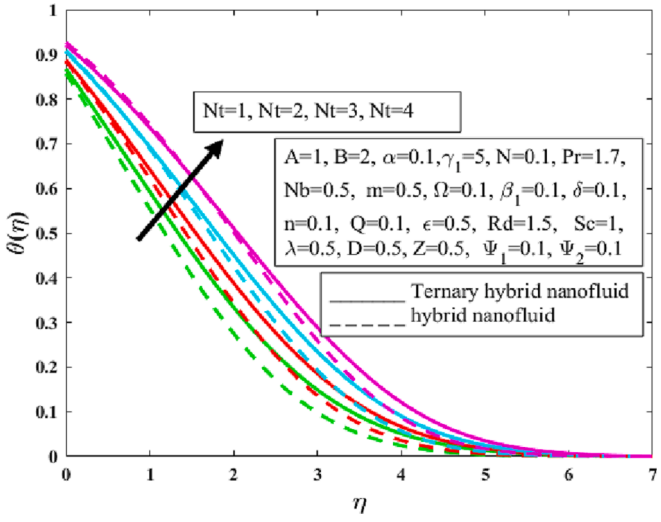


**Fig. 11.** Investigation of *Nt* given by [03*B*8]$(\eta)$.

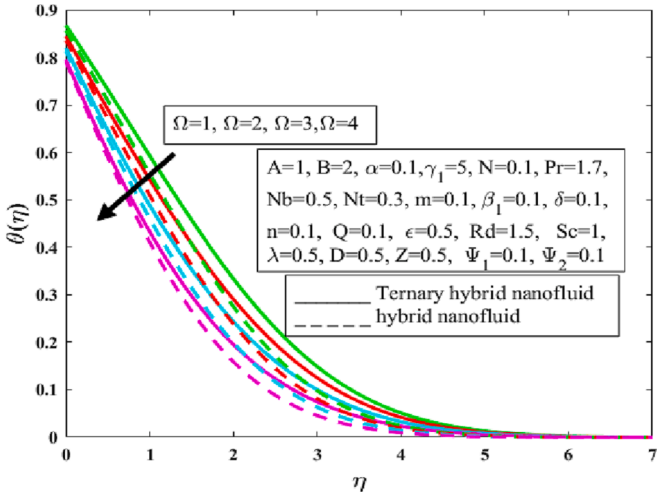


**Fig. 12.** Investigation of Ω arranged by [03*B*8]$(\eta)$.

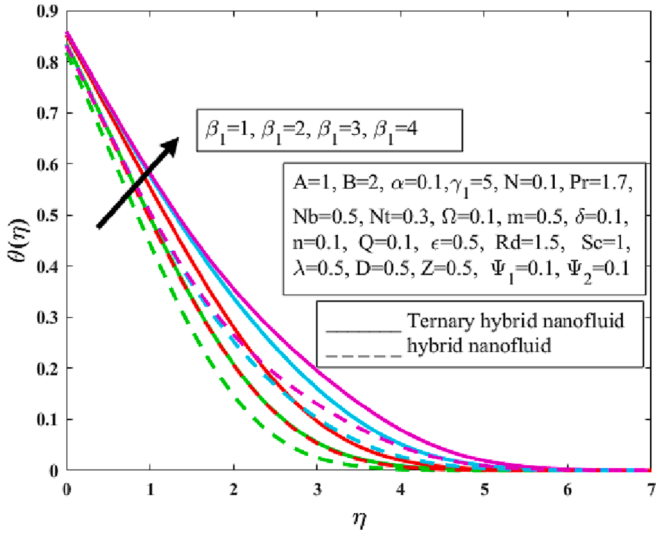


**Fig. 13.** Investigation of $\beta_1$ corresponds to [03*B*8]$(\eta)$.

$$\left.\begin{aligned} A_1 &= [(1-\phi_1)(1-\phi_2)(1-\phi_3)]^{-2.5}, \\ A_2 &= (1-\phi_3)\left\{(1-\phi_2)\left[\left[(1-\phi_1)+\phi_1\frac{\rho_1}{\rho_f}\right]\right]+\phi_2\frac{\rho_2}{\rho_f}\right\}+\phi_3\frac{\rho_3}{\rho_f}, \\ A_3 &= (1-\phi_3)\left\{(1-\phi_2)\left[(1-\phi_1)+\frac{(\rho C_p)_{s_1}}{(\rho C_p)_f}\phi_1\right]+\frac{(\rho C_p)_{s_2}}{(\rho C_p)_f}\phi_2\right\}+\frac{(\rho C_p)_{s_3}}{(\rho C_p)_f}\phi_3,\ A_4=\frac{k_{thnf}}{k_f} \end{aligned}\right\} \tag{15}$$

## Solution methodology

With the aid of restricted component computation, the corresponding limit conditions of the present model were mathematically reconstructed. The partition of the anticipated space into elements forms the foundation of the restricted component strategy (finite). This article examines the Galerkin finite element method (G-FEM) [40]. Fig. 2 serves as a reference for the limited component calculation's stream layout. This method has been applied to a few computational liquid elements (CFD) problems; the advantages of doing so are listed below.

**Step-I:** Solid structure (called ODEs) produces weak structure, and residuals are prearranged.
**Step-II:** To obtain a frail structure, outline capacities are directly extracted, and Galerkin limited component plot is applied.
**Step-III:** Building solidity components involves an assembly process, and a global firmness network is envisaged.
**Step-IV:** With the aid of the Picard linearization method, the algebraic outline (nonlinear conditions) is acquired.
**Step-V:** By manipulating the accompanying halting models and $10^{-5}$ (computational resistance), algebraic conditions are reenacted.

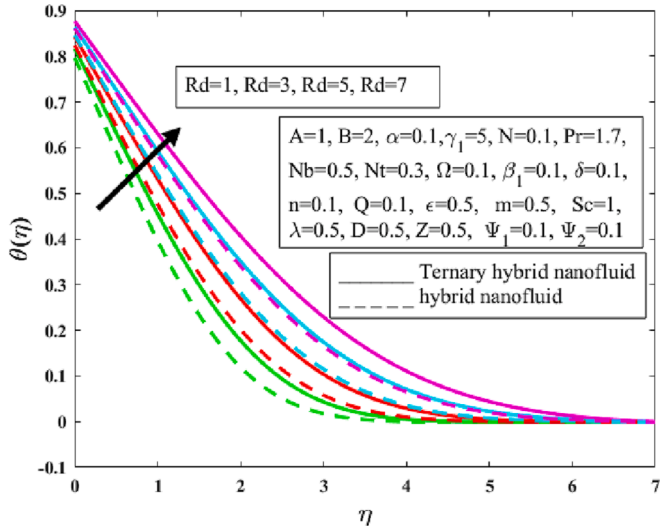


**Fig. 14.** Investigation of *Rd* formulated with respect to [03*B*8]($\eta$).

$\left|\frac{\eta_{i+1}-\eta_i}{\eta^i}\right| < 10^{-5}$.

Additionally, The Galerkin restricted module process's stream summary is shown in Fig. 3.

*Validation of code*

By contrasting the heat transport rate after the current process with the confirmed results of prior investigations, the validity of the computational technique was established [41,42]. Table 2 displays a comparison of recent research findings with those from earlier studies. The outcomes of the present exploration were quite exact and analogous.

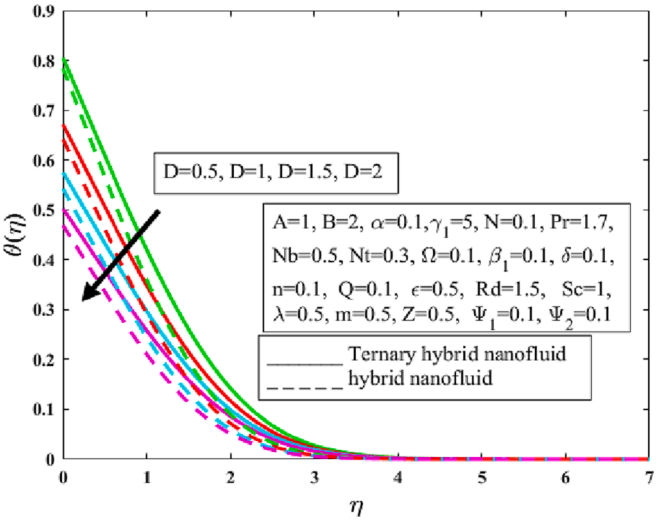


**Fig. 16.** Investigation of *D* arranged by [03*B*8]($\eta$).

## Results and discussion

The movement of Prandtl Eyring fluid disseminated with tri HNFs (*AA*7072, *AA7075*, *Ag*) through the deliberation of ethylene glycol by means of a base fluid with a modified Buongiorno HNF model. FEM a well-known numerical procedure, has been used to apply the mathematical model, which takes the form of nonlinear ODEs, to determine the solution. This study's major goal is to research how to increase heat transfer rate utilizing Ternary HNF as the primary emphasis, and it has been found that HNFs are better capable of doing so. The graphical findings that are included in the discussions part (Figs. 4-26) allow us a thorough assessment and examination of the numerical computations provided in the finite element method's segment on the approximate result.

Results show the impact of characterizing parameters, especially those that explain the novel aspects of the current study, such as the activation energy ($Q$), reaction rate constant ($\beta_1$), and endothermic/exothermic reaction parameter ($\Omega$). This is based on the assumption that

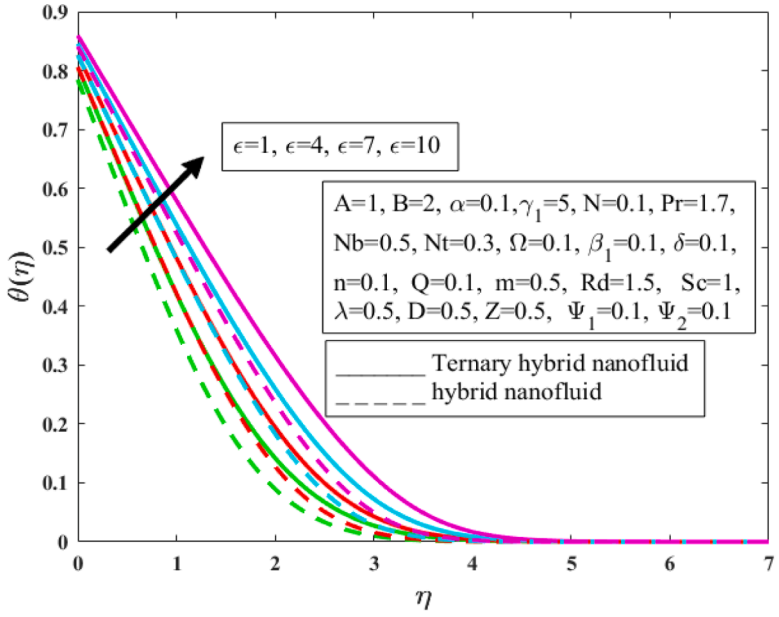


**Fig. 15.** Investigation of ϵ arranged by [03*B*8]($\eta$).

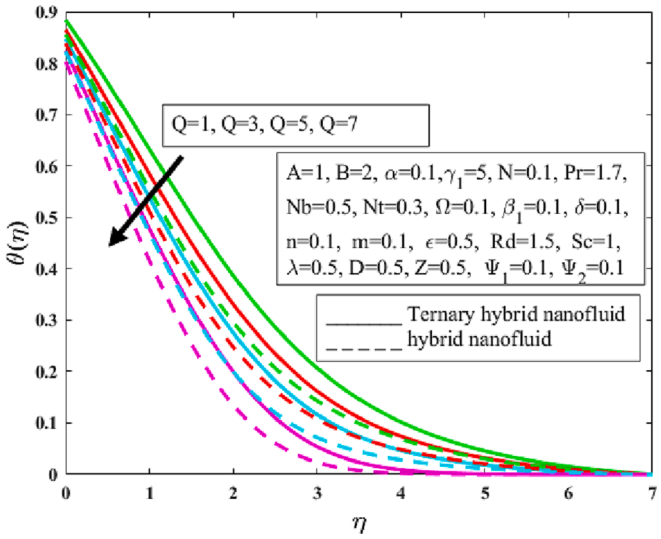


**Fig. 17.** Investigation of $Q$ with respect to.$[03B8](\eta)$.

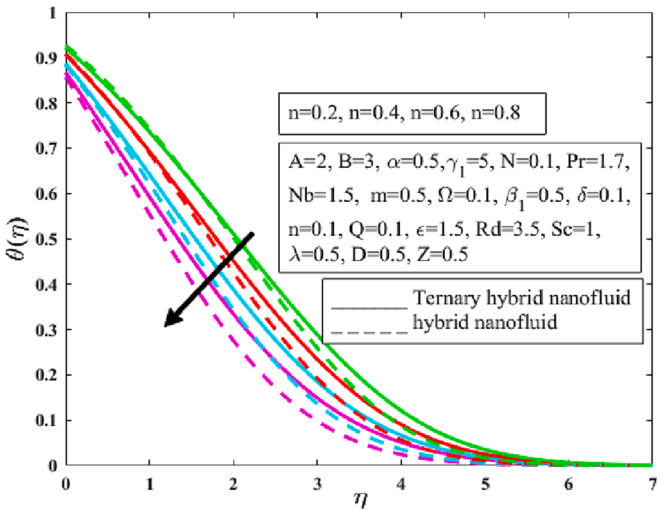


**Fig. 18.** Investigation of $n$ with admiration to $[03B8](\eta)$.

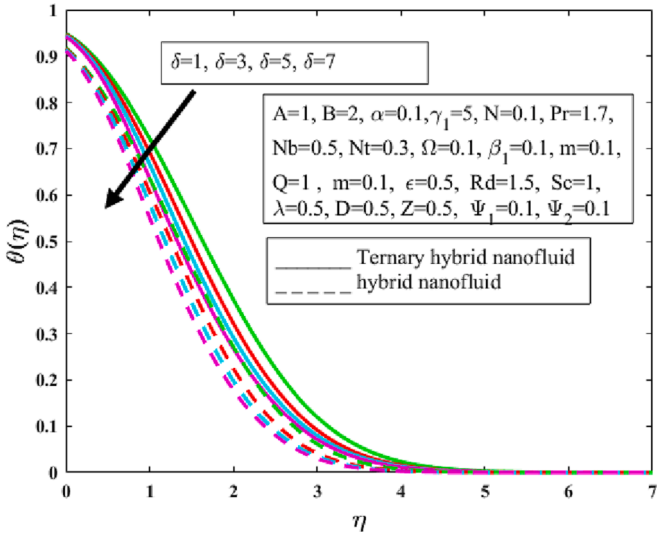


**Fig. 19.** Investigation of $\delta$ with reverence to $[03B8](\eta)$.

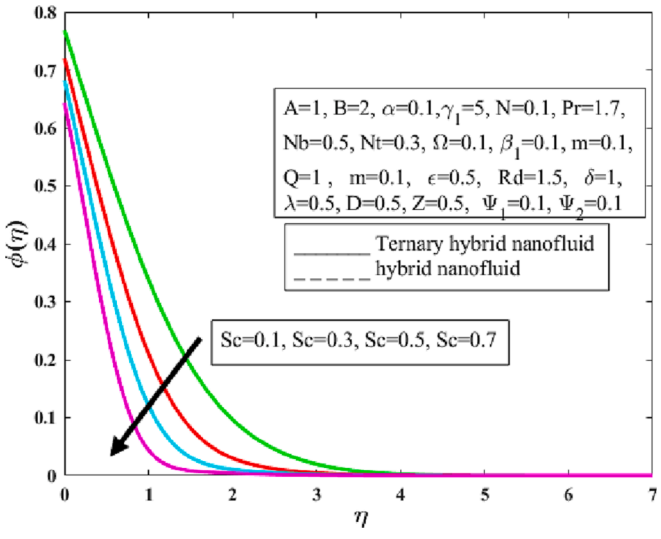


**Fig. 20.** Investigation of $Sc$ occurs with$\phi(\eta)$.

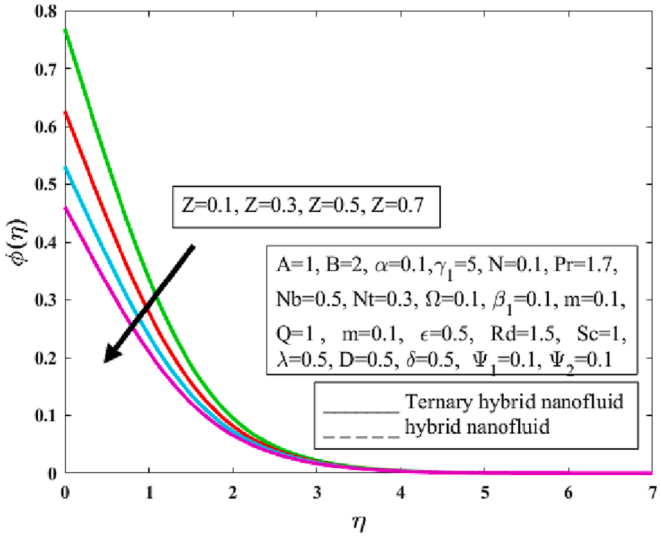


**Fig. 21.** Investigation of $Z$ occurs with $\phi(\eta)$.

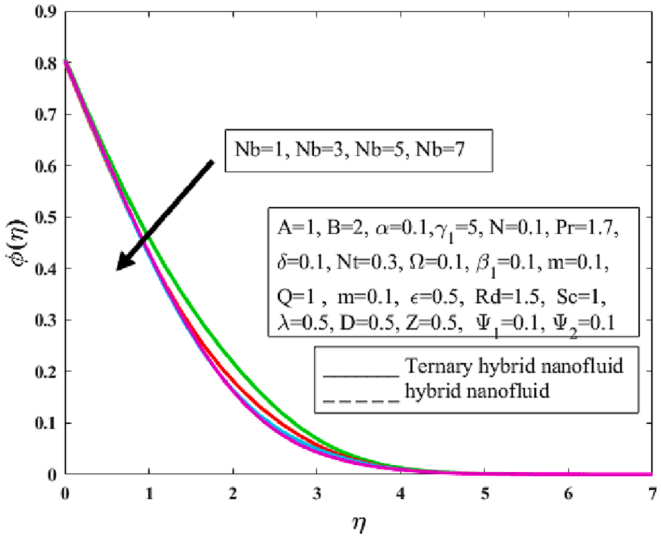


**Fig. 22.** Investigation of $Nb$ indicates with.$\phi(\eta)$.

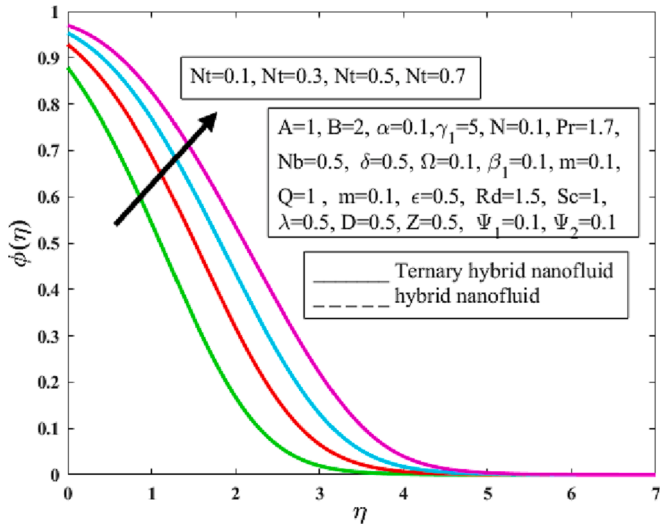


**Fig. 23.** Investigation of $Nt$ with respect to $\phi(\eta)$.

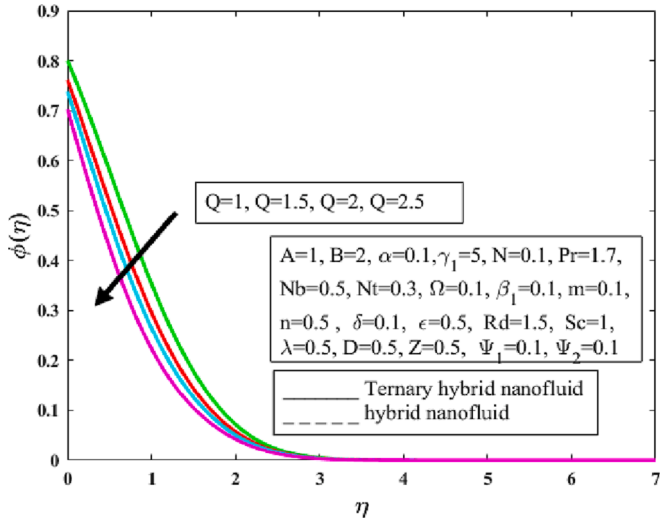


**Fig. 24.** Investigation of $Q$ on.$\phi(\eta)$.

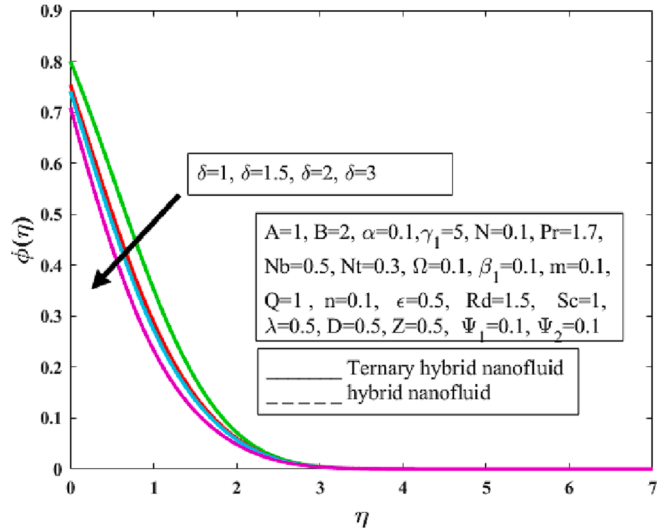


**Fig. 25.** Investigation of $\delta$ on $\phi(\eta)$.

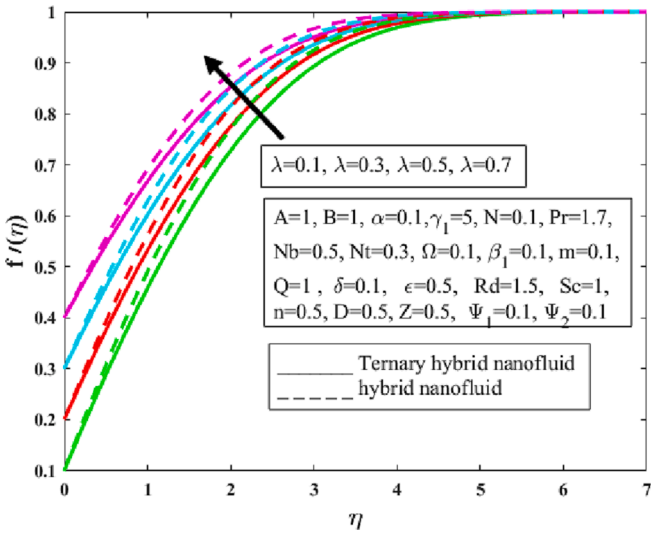


**Fig. 26.** Investigation of $\lambda$ on $\phi(\eta)$.

there are three diverse categories of nanoparticles. The speed, energy, and mass owing to stagnation point flow are all factors that the flow analysis takes into consideration.

Figs. 4-8 display the velocity distributions for various fluid parameters such as Prandtl liquid factor, elastic stricture, wedge constraint, wedge angle, and buoyancy parameter in both the cases like hybrid and ternary HNF. It is renowned from Fig. 4 that, with accumulative Prandtl fluid parameter the boundary layer thickness diminishes, results there is an increase in the velocity profile of nanofluids. Moreover, it is also noticed that higher velocities are found in the status of hybrid nanoliquid as compared with ternary hybridity nanoliquid. Physically fluid becomes less viscous under an amplification in $A$ which develops the velocity of liquid flow over stretching and elevates the velocity field $f'(\eta)$. The velocity increment is observed with the enhancement of the elastic parameter (see Fig. 5). It is reflected that liquid is transferring away from the vertical side in the upward path under magnification in elastic parameter $B$. Physically it is observed that the stretching capacity of the sheet magnifies owed to an enlargement in $B$ and less resistance is offered to a fluid moving over an expandable and the velocity of fluid amplifies which escalates $f'(\eta)$. It is noticed from Fig. 6 that, the rapidity rises with increasing amounts of wedge parameter. It is also noted that up to a certain distance, the velocity is higher for ternary hybrid nanofluids, later the same higher velocities are noticed for hybrid nanofluids. It is caused literally by the wedge parameter, which is connected to a pressure gradient. Higher wedge parameter values, therefore, suggest a beneficial pressure gradient that improves liquid movement. Additionally, for a higher value of $m$, the velocity distribution moves closer toward the edge's surface and opposing fluid movement. Additionally, the thickness in terms of momentum boundary layer increases with a positive change in m as well as decreases with the shear rate of the thickening fluid. It is depicted in Fig. 7 that, the wedge angle decreases the velocity of the nanofluid, and the trend in both the nanofluid is irregular. The velocity of the nanofluid declines with the rise of the buoyancy parameter (see Fig. 8). It is also investigated that, there is a mixed velocity behaviour for hybrid and ternary hybrid nanofluid based on the axial directions. Physically it is observed that a more viscous fluid generates less buoyancy and it is well established that the intersection of nanoparticles in the base fluid amplifies fluid density as well as viscosity and lessens buoyancy phenomenon as well as $f'(\eta)$.

Figs. 9-19 plotted to see the variations of nanoparticle temperature distributions for distinct parameters such as Prandtl number, Brownian diffusion parameter, thermophoresis parameter, endothermic/exothermic reactions parameter, reaction rate constant, radiation

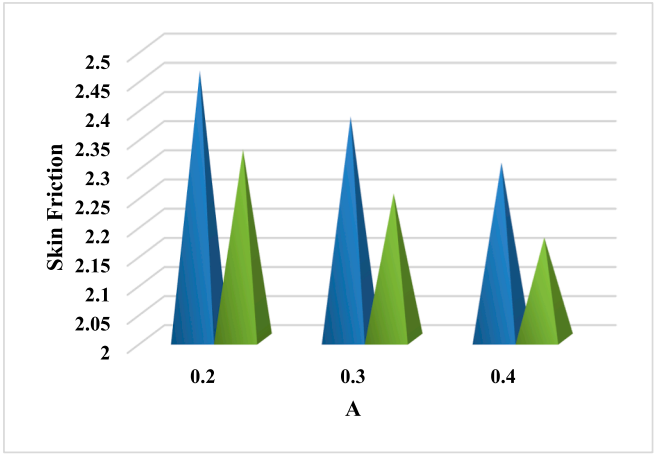


**Fig. 27.** Impact of Prandtl fluid parameter *A* on the surface drag coefficient. Blue lines represent ternary hybrid nanofluid and green lines represent di-hybrid nanofluid. (For interpretation of the references to colour in this figure legend, the reader is referred to the web version of this article.)

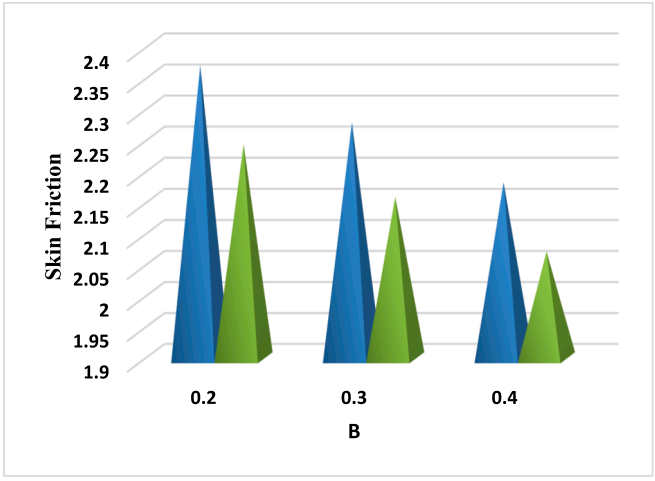


**Fig. 28.** Impact of elastic parameter *B* on the skin friction coefficient. Blue lines represent ternary hybrid nanofluid and green lines represent di-hybrid nanofluid. (For interpretation of the references to colour in this figure legend, the reader is referred to the web version of this article.)

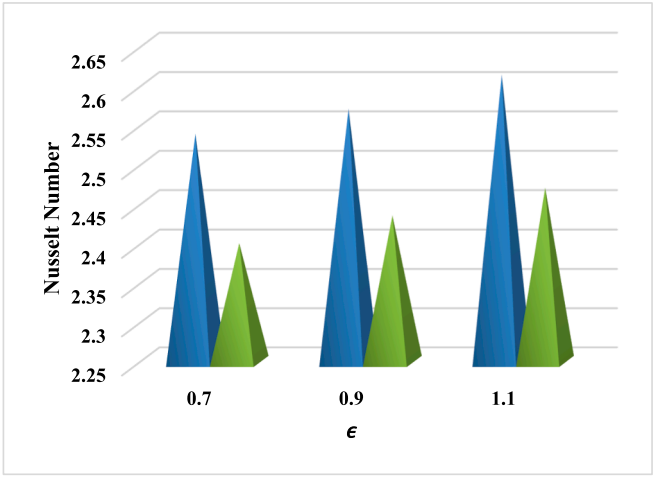


**Fig. 29.** Impact of thermal conductivity parameter ϵ on Nusselt number. Blue lines represent ternary hybrid nanofluid and green line represent di-hybrid nanofluid. (For interpretation of the references to colour in this figure legend, the reader is referred to the web version of this article.)

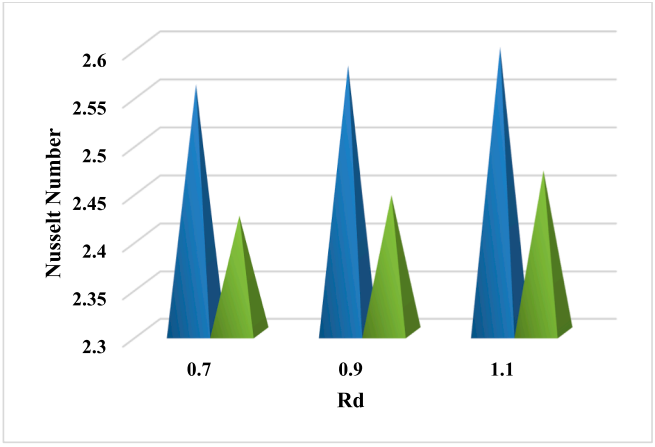


**Fig. 30.** Effect of thermal radiation *Rd* on Nusselt number. Blue lines represent ternary hybrid nanofluid and green lines represent di-hybrid nanofluid. (For interpretation of the references to colour in this figure legend, the reader is referred to the web version of this article.)

parameter, $\varepsilon$, convective heat flux, activation energy, power law index and the ratio of temperature. From Fig. 9, the stronger temperature boundary layer thickness is noticed with the enhancement in Prandtl number, results there is a decrement in the nanoparticle temperature of both the nanofluids. Moreover, the mixed kind of behaviour is noticed with respect to diverse values of the Prandtl number. Physically heat distributes more faster as a result of an enlargement in *Pr* which diminishes the heat transport phenomenon and temperature field $\theta(\eta)$. The rising Brownian diffusion parameter enhances the nanoparticle temperature of both nanofluids (see Fig. 10). Particles collide more at random because of magnification in *Nb*. Physically molecules are more random and share more kinetic energy with each other which eventually amplifies the thermal conductivity of the fluid. As a result heat transfer among the liquid particles amplify and temperature field $\theta(\eta)$. It is obvious from Fig. 11 that, the nanomolecules temperature growths with stronger thermophoresis restriction. Physically molecules from the hotter region to the colder region by rising Nt and the equilibrium condition is maintained. After some time the temperature of the fluid amplifies by improving *Nt* with amplifies $\theta(\eta)$. It is concluded from Fig. 12 that, endothermic reaction decreases the nanoparticle temperature of both nanofluids. It is observed that energy is released or absorbed during the chemical reaction process. During the endothermic reaction, energy is absorbed by the system which later on decreases the temperature of the fluid and $\theta(\eta)$. The reaction rate constant enhances the temperature profile (see Fig. 13). Because there are more successful interactions between reactants as a result of the elevated temperature, the rate at which they react rises. The total amount of molecules containing energy equivalent to or even above the energy of activation rises when the temperature rises. As a result, both the reaction's pace and the total number of efficient collisions rise. It is depicted from the graph that, the nanomolecules temperature rises with enhancing radiation parameter (see Fig. 14), and a similar trend is noticed with ϵ (see Fig. 15). The inclusion of nanomolecules in standard liquid absorbs more radiation in contrast to simple fluid. Physically, thermal radiative fluxing is operated where significant heat is required. More heat is delivered to a system by rising *Rd* which amplifies the temperature inside the fluid and eventually amplifies $\theta(\eta)$. Particles collide more freely and share more kinetic energy with each other as a result of magnification in ϵ. Insertion of nanoparticles in the liquid develops its thermal conductance phenomenon and furthermore improves $\theta(\eta)$. It is perceived from Fig. 16 that, with the enhancing convective heat flux, the nanoparticle

**Table 3**
Investigation of varied dimensionless factors on the frictional force factor.

| $A$ | $B$ | $m$ | $\gamma_1$ | $N$ | $\vartheta$ | $\lambda$ | $C_{fx}Re_x^{1/2}$ |
|---|---|---|---|---|---|---|---|
| 0.5 | 3 | 1 | 5 | 0.1 | 0.1 | 0.5 | 1.1412 |
| 0.8 | | | | | | | 1.2517 |
| 1.1 | | | | | | | 1.4116 |
| 1.5 | | | | | | | 1.6901 |
| | 4 | | | | | | 1.1615 |
| | 5 | | | | | | 1.3412 |
| | 6 | | | | | | 1.5854 |
| | | 1.2 | | | | | 1.2119 |
| | | 1.4 | | | | | 1.5467 |
| | | 1.6 | | | | | 1.7089 |
| | | | 6 | | | | 0.9907 |
| | | | 7 | | | | 0.8576 |
| | | | 8 | | | | 0.6431 |
| | | | | 0.3 | | | 0.9000 |
| | | | | 0.5 | | | 0.7895 |
| | | | | 0.7 | | | 0.5521 |
| | | | | | 0.3 | | 0.6767 |
| | | | | | 0.5 | | 0.4003 |
| | | | | | 0.7 | | 0.2958 |
| | | | | | | 0.6 | 0.8324 |
| | | | | | | 0.65 | 0.6217 |
| | | | | | | 0.7 | 0.4797 |

temperature declines in both the nanofluids. The nanoparticle temperature reduces with increasing values of activation energy (see Fig. 17). This is because there are more particles with the necessary minimum energy. As the temperature drops, the response rate drops as well. The activation energy is unaffected by temperature changes. Catalyst addition is the sole means to change the activation energy. It is noted from Figs. 18-19 that, with the enhancing power law index and temperature ratio, the nanoparticle temperature decreases in both the nanofluids. Moreover, from these nanoparticle temperature pictorial notations, it is detected that the higher temperature is seen in the ternary HNF case as compared with the simple hybrid nanofluid case. Physically viscosity is inversely linked with temperature. Viscous fluids have more viscosity and low temperatures. It is also observed that a positive change in temperature decreases viscosity. More resistance is offered to the fluid flow subjected to an incremental change in n which lessens $\theta(\eta)$. The temperature ratio parameter is the ratio of free stream temperature to wall temperature. When the difference between a free stream and wall temperature increases, heat transfer inside the fluid diminishes, and $\theta(\eta)$ decreases.

Figs. 20-26 are drawn to see the effect of diverse parameters such as Schmidt number, convective mass flux, Brownian diffusion parameter, thermophoresis parameter, activation energy, temperature ratio, and

**Table 4**
Change of distinguished variables on the heat transport and mass transport rates.

| $\epsilon$ | $Rd$ | $Pr$ | $Nb$ | $Nt$ | $\Omega$ | $\beta_1$ | $\delta$ | $n$ | $Q$ | $Sc$ | $Z$ | $\Psi_1$ | $\Psi_2$ | $Nu_xRe_x^{1/2}$ | $Sh_xRe_x^{1/2}$ |
|---|---|---|---|---|---|---|---|---|---|---|---|---|---|---|---|
| 1 | 1 | 1.7 | 1 | 0.5 | 0.1 | 0.1 | 0.1 | 0.1 | 0.1 | 0.5 | 0.5 | 0.1 | 0.1 | 1.4213 | 0.6521 |
| 2 | | | | | | | | | | | | | | 1.3154 | 0.6621 |
| 3 | | | | | | | | | | | | | | 1.2001 | 0.6798 |
| 4 | | | | | | | | | | | | | | 1.0957 | 0.6851 |
| | 2 | | | | | | | | | | | | | 1.3157 | 0.6891 |
| | 3 | | | | | | | | | | | | | 1.6041 | 0.6901 |
| | 4 | | | | | | | | | | | | | 1.8711 | 0.6998 |
| | | 3 | | | | | | | | | | | | 1.3890 | 0.6690 |
| | | 4 | | | | | | | | | | | | 1.4771 | 0.6692 |
| | | 5 | | | | | | | | | | | | 1.4982 | 0.6699 |
| | | | 2 | | | | | | | | | | | 1.2312 | 0.6851 |
| | | | 3 | | | | | | | | | | | 1.1301 | 0.6721 |
| | | | 4 | | | | | | | | | | | 1.0015 | 0.6530 |
| | | | | 1 | | | | | | | | | | 1.1576 | 0.5432 |
| | | | | 1.5 | | | | | | | | | | 0.9742 | 0.4576 |
| | | | | 2 | | | | | | | | | | 0.9063 | 0.3211 |
| | | | | | 0.3 | | | | | | | | | 1.2115 | 0.6104 |
| | | | | | 0.5 | | | | | | | | | 1.0143 | 0.6233 |
| | | | | | 0.7 | | | | | | | | | 0.8665 | 0.6402 |
| | | | | | | 0.3 | | | | | | | | 1.4300 | 0.5001 |
| | | | | | | 0.5 | | | | | | | | 1.3114 | 0.5155 |
| | | | | | | 0.7 | | | | | | | | 1.2197 | 0.5214 |
| | | | | | | | 0.3 | | | | | | | 1.1231 | 0.5321 |
| | | | | | | | 0.5 | | | | | | | 1.2151 | 0.5376 |
| | | | | | | | 0.7 | | | | | | | 1.2465 | 0.5454 |
| | | | | | | | | 0.3 | | | | | | 1.5621 | 0.5552 |
| | | | | | | | | 0.5 | | | | | | 1.5670 | 0.5709 |
| | | | | | | | | 0.7 | | | | | | 1.5695 | 0.5963 |
| | | | | | | | | | 0.3 | | | | | 1.4867 | 0.6176 |
| | | | | | | | | | 0.5 | | | | | 1.4415 | 0.6021 |
| | | | | | | | | | 0.7 | | | | | 1.4312 | 0.5876 |
| | | | | | | | | | | 1 | | | | 1.3521 | 0.4105 |
| | | | | | | | | | | 1.5 | | | | 1.3426 | 0.4788 |
| | | | | | | | | | | 2 | | | | 1.3311 | 0.5459 |
| | | | | | | | | | | | 1 | | | 1.5432 | 0.5431 |
| | | | | | | | | | | | 1.5 | | | 1.5839 | 0.5002 |
| | | | | | | | | | | | 2 | | | 1.6277 | 0.4875 |
| | | | | | | | | | | | | 0.2 | | 1.2176 | 0.6631 |
| | | | | | | | | | | | | 0.3 | | 1.0213 | 0.6754 |
| | | | | | | | | | | | | 0.4 | | 0.9966 | 0.6885 |
| | | | | | | | | | | | | | 0.2 | 1.1759 | 0.6021 |
| | | | | | | | | | | | | | 0.3 | 1.1021 | 0.5730 |
| | | | | | | | | | | | | | 0.4 | 0.9977 | 0.5411 |

moving wedge parameter. It is noted from Fig. 20 that, the nanoparticle attentiveness decreases with rising values of the Schmidt number, where the concentration boundary layer thickness is stronger with the Schmidt number. Schmidt number is thermal to mass diffusivity. Physically mass diffuses more quickly by improving *Sc* which lessens *Sc*. The nanoparticle concentration decreases with convective mass flux (see Fig. 21), and a similar trend is noticed with rising Brownian diffusion parameter (see Fig. 22). It is declared that the concentricity of the liquid diminishes as a result of magnification in mass flux through convection which diminishes $\phi(\eta)$. Physically concentration is changed with temperature. The concentration of the product decreased and the concentration of the reactants rose as the temperature rose. That is why a frequent collision in *Nb* amplifies fluid temperature but diminishes concentration field $\phi(\eta)$. It is depicted in Fig. 23 that, the nanoparticle concentration enhances with rising values of thermophoresis parameter. Physically particles of the liquid migrate from the hotter zone to the colder plane which amplifies the concentricity of the species within the liquid and eventually amplifies $\phi(\eta)$. Activation energy decreases the nanoparticle concentration (see Fig. 24). A catalyst lowers the reaction's transition state, lowering the reaction's activation energy in the process. As a result $\phi(\eta)$ diminishes. Clearly, from Fig. 25, the temperature ratio increases the nanoparticle concentration decreases. It is observed that the mass diffusion phenomenon diminishes when the change between surface and ambient temperature grows which diminishes the rate of mass transport and $\phi(\eta)$. It is detected from Fig. 26 that, the moving wedge variable boosts the nanoparticle concentration. Physically an amplification in the wedge parameter provides less resistance to the fluid flow and the mass diffusion rate amplifies which brings about an amplification in $\phi(\eta)$. Figs. 27-28 sketched the impact of the Prandtl fluid parameter *A* and elastic parameter *B* on the surface drag coefficient. It is moderately apparent a confident change in *A* magnifies the viscosity phenomenon and provides more resistance to the fluid flow which actually amplifies the friction phenomenon and provides more drag to the fluid flow and furthermore diminishes the skin friction phenomenon. It is noticed that magnification in *B* provides an extension in the stretching sheet and more resistance is offered to fluid flow and the drag phenomenon amplifies which diminishes surface drag friction. Figs. 29-30 are designed to explore the influence of thermal conductivity $\in$ and thermal radiation *Rd* on heat transfer Nusselt number. It is quite evident that particles collide more randomly under the magnification in temperature and share more kinetic energy with each and escalates $\in$ and heat transfer rate. Electromagnetic waves are really the means through which radiation is transmitted. When these waves interact with a liquid, they raise the temperature of the substance. Because of this, a magnification *Rd* increases the rate of heat transmission. Temperature escalates more in the situation of tri hybridity nanoliquid in comparison with di HNFs.

Table 3 displays the skin friction coefficient variations for diverse parameters such as Prandtl fluid factor, elastic constraint, wedge restriction, buoyancy parameter, *N*, wedge angle, and moving wedge parameter. It is spotted that the frictional force factor raises with rising values of the Prandtl fluid parameter, elastic parameter, and wedge parameter, and the trend is reversed with enhancing parameters such as buoyancy parameter *N*, wedge angle and moving wedge parameter. Table 4 represents the variations in heat transfer rate and mass transition rate with particular to diverse fluid parameters. It is observed that both the heat and mass transference rates enhances with increasing radiation parameter, temperature ratio, power law index, and activation energy, and the converse path is detected in the case of thermophoresis variable and reaction rate constant. Increasing values $\in$ decreases the heat transport rate, while it expands the mass transmission rate. Prandtl number develops the heat transfer rate and declines the mass transfer rate. Heat transfer rate decreases with increasing Brownian diffusion parameter, endothermic/exothermic reaction, and Schmidt number, while with these parameters the mass transfer rate enhances. Convective mass flux improves the heat transfer frequency and drops the mass transfer amount. Heat transfer diminishes but the Sherwood number amplifies in the case of the thermal relaxation parameter $\Psi_1$ but both heat transfer and Sherwood number diminishes owing to magnification in concentration relaxation parameter$\Psi_2$.

## Concluding remarks

With ethylene glycol as a standard liquid and consideration of multiple physical parameters, the study piece investigates the steady flowing of Prandtl Eyring liquid discrete with tri HNFs. The Modified Buongiorno prototype is operated to jointly examine Brownian motion, thermophoresis, and their impacts. The numerical approach (i.e., FEM) is applied to calculate the ascending non-dimensional boundary value problem. A comprehensive parametric examination of the appearances of distinct parameters is shown. The subsequent conclusions are drawn:

- The resulting velocity was growing by an increase in $A, B$ and $m$, while inclination, as well as buoyancy parameters, have reverse outcomes on this.
- The temperatures with the thickener of the thermal boundary layer decrease on an enhancing $Pr, Nb, \Omega, D, Q, n$ and $\delta$ parameters simultaneously.
- Liquid temperature enhances with mounting in $Nt, \beta_1, \in$ and $Rd$ quantities.
- Species concentration of fluid was reduced by an increase through Schmidt quantity as well as activation energy parameter.
- It is discovered that the temperature in the ternary hybridity nanofluid case is greater than in the simple hybrid nanofluid case.
- Wedge parameter helps us to improve the friction factor.
- Thermal radiation and activation energy contribute to higher Nusselt and Sherwood numbers.
- Heat transfer phenomenon diminishes as a result of a magnification in thermal relaxation time.
- A positive variation in the concentration relaxation parameter diminishes the Sherwood number.

### *Future direction*

In the present article, a novel modified Buongiorno ternary hybrid nanofluid simulation has been in order to investigate the influence t of nanomolecules on fluid flow subjected to a wedge. In the future, this work has been utilized in order to develop a modified Buongiorno tetra hybrid nanofluid model to probe the effect of tetra nanomaterials on the fluid over various geometries like disks, cylinders, nonlinear expandable sheets, needles, etc. It can be said that in the near future we are currently working on extending the current concept in this study to include the main ideas in the following valuable papers [43–45].

## Declaration of Competing Interest

The authors declare that they have no known competing financial interests or personal relationships that could have appeared to influence the work reported in this paper.

## Data availability

Data will be made available on request.

## Acknowledgement

The authors extend their appreciation to the Deanship of Scientific Research at King Khalid University for funding this work through Large groups (project under grant number RGP. 2/108/43).

## References


[1] Shahzad MH, Nadeem S, Awan AU, Allahyani SA, Ahammad NA, Eldin SM. On the steady flow of non-Newtonian fluid through multi-stenosed elliptical artery: A theoretical model. Ain Shams Eng J 2023:102262. https://doi.org/10.1016/j.asej.2023.102262.

[2] Raza N, Nauman AK, Khan AU, Awan KAA. Dynamical aspects of transient electro-osmotic flow of Burgers' fluid with zeta potential in cylindrical tube. Nonlinear Eng 2023;12:20220256.

[3] Shahzad MH, Awan AU. Mechanics of heated Rabinowitsch fluid in elliptic vertical duct: Peristalsis and analytical study. Int J Mod Phys B 2023:2350274. https://doi.org/10.1142/S0217979223502740.

[4] Shahzad, Muhammad Hasnain and Awan, Aziz Ullah, Non-Newtonian characteristics of blood flow in a multi-stenosed elliptical artery: A case of sensitivity analysis, *International Journal of Modern Physics B*, 37(2023)2350182}.

[5] Aziz Ullah Awan, N. Ameer Ahammad, Wasfi Shatanawi, Seham Ayesh Allahyani, ElSayed M. Tag-ElDin, Nadeem Abbas, Bagh Ali, Significance of magnetic field and Darcy–Forchheimer law on dynamics of Casson-Sutterby nanofluid subject to a stretching circular cylinder, *International Communications in Heat and Mass Transfer* 139 (2022) 106399.

[6] Syed Asif Ali Shah, N. Ameer Ahammad, Bagh Ali, Kamel Guedri, Aziz Ullah Awan, Fehmi Gamaoun, ElSayed M. Tag-ElDin, Significance of bio-convection, MHD, thermal radiation and activation energy across Prandtl nanofluid flow: A case of stretching cylinder, *International Communications in Heat and Mass Transfer*137 (2022) 106299.

[7] Awan AU, Majeed S, Ali B, Ali L. Sonia Majeed, Bagh Ali, Liaqat Ali, Significance of nanoparticles aggregation and Coriolis force on the dynamics of Prandtl nanofluid: The case of rotating flow. Chin J Phys 2022;79:264–74.

[8] Shah NA, Awan AU, Khan R, Tlili I, Farooq MU, Salah B, et al. Free convection Hartmann flow of a viscous fluid with damped thermal transport through a cylindrical tube. Chinese J Phys 2022;80:19–33.

[9] Shuguang Li, M. Ijaz Khan, Faris Alzahrani, Sayed M. Eldin, Heat and mass transport analysis in radiative time dependent flow in the presence of Ohmic heating and chemical reaction, viscous dissipation: An entropy modeling, *Case Studies in Thermal Engineering*, 42 (2023) 102722.

[10] Zhimeng Liu, Shuguang Li, Tooba Sadaf, Sami Ullah Khan, Faris Alzahrani, M. Ijaz Khan, Sayed M. Eldin, Numerical bio-convective assessment for rate type nanofluid influenced by Nield thermal constraints and distinct slip features, *Case Studies in Thermal Engineering* 44 (2023) 102821.

[11] Chu Y-M, Jakeer S, Reddy SRR, Rupa ML, Trabelsi Y, Khan MI, et al. Double diffusion effect on the bio-convective magnetized flow of tangent hyperbolic liquid by a stretched nano-material with Arrhenius Catalysts. Case Stud Thermal Eng 2023;44:102838.

[12] Li, Shuguang, Ali, Farhan, Zaib, A., Loganathan, K., Eldin, Sayed M. and Ijaz Khan, M., Bioconvection effect in the Carreau nanofluid with Cattaneo–Christov heat flux using stagnation point flow in the entropy generation: Micromachines level study, *Open Physics*, 21(2023)20220228.

[13] Li S, Raghunath K, Alfaleh A, Ali F, Zaib A, Khan MI, et al. Effects of activation energy and chemical reaction on unsteady MHD dissipative Darcy-Forchheimer squeezed flow of Casson fluid over horizontal channel. Sci Rep 2023;13(1).

[14] Li S, Puneeth V, Saeed AM, Singhal A, Al-Yarimi FAM, Khan MI, et al. Analysis of the Thomson and Troian velocity slip for the flow of ternary nanofluid past a stretching sheet. Sci Rep 2023;13(1).

[15] Xin, Xiao, Khan, Muhammad Ijaz and Li, Shuguang, Scheduling equal-length jobs with arbitrary sizes on uniform parallel batch machines, *Open Mathematics*, 21 (2023)20220562.

[16] Jahanshahi H, Yao Q, Ijaz Khan M, Moroz I. Muhammad Ijaz Khan, Irene Moroz, Unified neural output-constrained control for space manipulator using tan-type barrier Lyapunov function. Adv Space Res 2023;71(9):3712–22.

[17] Mamatha SU, Devi RR, Ahammad NA, Shah NA, Rao BM, Raju CSK, et al. Guedri Multi-linear regression of triple diffusive convectively heated boundary layer flow with suction and injection: lie group transformations Int. J Modern Phys B 2023;37 (01):2350007.

[18] Kiranakumar. H. V, Thejas R, Naveen C S *et al.* A review on electrical and gas-sensing properties of reduced graphene oxide-metal oxide nanocomposites. *Biomass Conv. Bioref.* (2022).

[19] Anuar, N. S., Bachok, N., Arifin, N. M., & Rosali, H. (2021). Analysis of Al2O3-Cu nanofluid flow behaviour over a permeable moving wedge with convective surface boundary conditions. Journal of King Saud University-Science, 33(3), 101370.

[20] Mishra P, Acharya MR, Panda S. Mixed convection MHD nanofluid flow over a wedge with temperature-dependent heat source. Pramana 2021;95(2):1–12.

[21] Khan WA, Pop I. Boundary Layer Flow Past a Wedge Moving in a Nanofluid. Math Probl Eng 2013;2013:1–7.

[22] Dharmaiah G, Dinarvand S, Balamurugan KS. MHD radiative ohmic heating nanofluid flow of a stretching penetrable wedge: A numerical analysis. Heat Transfer 2022;51(5):4522–43.

[23] Sarkar S, Endalew MF. Effects of melting process on the hydromagnetic wedge flow of a Casson nanofluid in a porous medium. Boundary Value Problems 2019;2019 (1):1–14.

[24] Khan M, Azam M, Alshomrani AS. Unsteady slip flow of Carreau nanofluid over a wedge with nonlinear radiation and new mass flux condition. Results Phys 2017;7: 2261–70.

[25] Madhu M, Reddy CS, Kishan N. Magnetohydrodynamic flow and heat transfer to Sisko nanofluid over a wedge. Int J Fluid Mech Res 2017;44(1):1–13.

[26] Kebede, T., Haile, E., Awgichew, G., & Walelign, T. (2020). Heat and mass transfer analysis in unsteady flow of tangent hyperbolic nanofluid over a moving wedge with buoyancy and dissipation effects. Heliyon, 6(4), e03776.

[27] Rajput S, Verma AK, Bhattacharyya K, Chamkha AJ. Unsteady nonlinear mixed convective flow of nanofluid over a wedge: Buongiorno model. Waves Random Complex Media 2021:1–15.

[28] Madhu M, Kishan N. MHD flow and heat transfer of Casson nanofluid over a wedge. Mechanics & Industry 2017;18(2):210.

[29] Jabeen K, Mushtaq M, Akram Muntazir RM. Suction and injection impacts on Casson nanofluid with gyrotactic micro-organisms over a moving wedge. J Fluids Eng 2022;144(1).

[30] Dinarvand S, Rostami MN, Pop I. A novel hybridity model for TiO2-CuO/water hybrid nanofluid flow over a static/moving wedge or corner. Sci Rep 2019;9(1): 1–11.

[31] Zainal NA, Nazar R, Naganthran K, Pop I. Flow and heat transfer over a permeable moving wedge in a hybrid nanofluid with activation energy and binary chemical reaction. Int J Numer Meth Heat Fluid Flow 2021.

[32] Kakar, N., Khalid, A., Al-Johani, A. S., Alshammari, N., & Khan, I. (2022). Melting heat transfer of a magnetized water-based hybrid nanofluid flow past over a stretching/shrinking wedge. Case Studies in Thermal Engineering, 30, 101674.

[33] Zainal NA, Nazar R, Naganthran K, Pop I. Stability Analysis of Unsteady Hybrid Nanofluid Flow over the Falkner-Skan Wedge. Nanomaterials 2022;12(10):1771.

[34] Berrehal H, Dinarvand S, Khan I. Mass-based hybrid nanofluid model for entropy generation analysis of flow upon a convectively-warmed moving wedge. Chin J Phys 2022;77:2603–16.

[35] Ogunniyi, P. O., Gbadeyan, A. J., Agarana, M. C., & Yusuf, T. A. Nonlinear thermal radiation on MHD tangential hyperbolic hybrid nanofluid over a stretching wedge with convective boundary condition. Heat Transfer.

[36] Waini I, Ishak A, Pop I. MHD flow and heat transfer of a hybrid nanofluid past a permeable stretching/shrinking wedge. Appl Math Mech 2020;41(3):507–20.

[37] Roşca NC, Roşca AV, Pop I. Mixed convection flow of a hybrid nanofluid past a vertical wedge with thermal radiation effect. Int J Numer Meth Heat Fluid Flow 2021.

[38] Basha HT, Sivaraj R, Animasaun IL. Stability analysis on Ag-MgO/water hybrid nanofluid flow over an extending/contracting Riga wedge and stagnation point. Comput Thermal Sci: Int J 2020;12(6).

[39] Hassan M, Faisal A, Ali I, Bhatti MM, Yousaf M. Effects of Cu–Ag hybrid nanoparticles on the momentum and thermal boundary layer flow over the wedge. Proc Inst Mech Eng, Part E: J Process Mech Eng 2019;233(5):1128–36.

[40] Hou E, Wang F, Nazir U, Sohail M, Jabbar N, Thounthong P. Dynamics of tri-hybrid nanoparticles in the rheology of pseudo-plastic liquid with Dufour and Soret effects. Micromachines 2022;13(2):201.

[41] Das S, Chakraborty S, Jana RN, Makinde OD. Entropy analysis of unsteady magneto-nanofluid flow past accelerating stretching sheet with convective boundary condition. Appl Math Mech 2015;36(2):1593–610.

[42] Bouslimi J, Alkathiri AA, Alharbi AN, Jamshed W, Eid MR. Dynamics of Convective Slippery Constraints on Hybrid Sutterby Nanofluid Flow by Employing Galerkin Finite Element Simulation in a Porous Material. Nanotechnol Rev 2022;11: 1219–36.

[43] W. Jamshed, M. R. Eid, S. M. Hussain, A. Abderrahmane, R. Safdar, O. Younis, A. A. Pasha, Physical specifications of MHD mixed convective of Ostwald-de Waele nanofluids in a vented-cavity with inner elliptic cylinder, International Communications in Heat and Mass Transfer, vol. 134, pp. 106038, 2022.

[44] F. Fangfang, T. Sajid, W. Jamshed, M. R. Eid, G. C. Altamirano, I. Altaf, A. Abd-Elmonem, S. M. El Din, Thermal transport and characterized flow of trihybridity Tiwari and Das Sisko nanofluid via a stenosis artery: A case study, Case Studies in Thermal Engineering, vol. 47, pp. 103064, 2023.

[45] Hanif H, Jamshed W, Devi SU, Eid MR, Shafie S, Ibrahim RW, Mohd Nasir NAA, Abd-Elmonem A, El Din SM. Thermal description and entropy evaluation of magnetized hybrid nanofluid with variable viscosity via Crank-Nicolson method. Case Studies Therm Eng 2023;47:103132.